Nanoscale

Accepted Manuscript

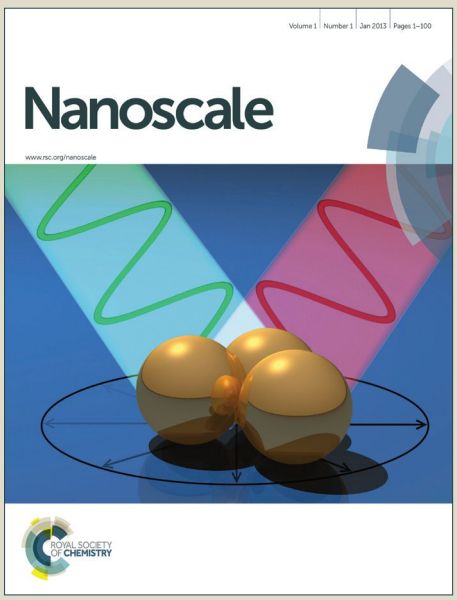

ROYAL SOCIETY OF CHEMISTRY

www.rsc.org/nanoscale

Nanoscale

Article

Growth of multiple WS_2 /SnS layered semiconductor heterojunctions

Received 00th January 20xx,
Accepted 00th January 20xx

DOI: 10.1039/x0xx00000x

www.rsc.org/

Robert Browning[a], Paul Plachinda[a], Prasanna Padigi[a], Raj Solanki[a], and Sergei Rouvimov[b]

Both WS_2 and SnS are 2-dimensional, van der Waals semiconductors, but with different crystal structures. Heteroepitaxy of these materials was investigated by growing 3 alternating layers of each of these materials using atomic layer deposition on 5 cm x 5 cm substrates. Initially, WS_2 and SnS films were grown and characterized separately. Back-gated transistors of WS_2 displayed n-type behavior with an effective mobility of 12 $cm^2 V^{-1} s^{-1}$, whereas SnS transistors showed a p-type conductivity with a hole mobility of 818 $cm^2 V^{-1} s^{-1}$.All mobility measurements were performed at room temperature. As expected, the heterostructure displayed an ambipolar behavior with a slightly higher electron mobility than that of WS_2 transistors, but with a significantly reduced hole mobility. The reason for this drop can be explained with transmission electron micrographs that show the striation direction of the SnS layers is perpendicular to that of the $WS_2$with a 15 degree twist, hence the holes have to pass through van der Waals layers that results in drop of their mobility.

Introduction

The unique electrical, thermal, and spin properties of two-dimensional (2D) materials, such as transition metal chalcogenides, are derived from the nature of their atomic bonds. Within each 2D layer, the metal and chalcogenide atoms are held by covalent-ionic mixed bonds and the individual layers are held together by van der Waals bonds[1, 2]. Over the past few years, a significant number of articles have been published on properties of single and few-layered films of semiconducting (e.g., MoS_2), conducting (e.g., TiS_2), and insulating (e.g., BN) 2D crystals[1-3]. To utilize these materials for fabrication of devices, one would need to produce electrically modulated layers which can be achieved either by doping or via selecting intrinsically doped layers for producing heterojunctions. However, at this time identification of suitable dopants is lagging for these materials, hence heterojunctions are being utilized to achieve this goal. Since single layers have no dangling bonds, van der Waals heterostructures formed by stacking these layers should, in principle, be free of lattice matching constraints and interface states that should lead to high performance devices. Moreover, first-principle density functional calculations of the metal chalcogenide heterojunctions predict unique properties such as formation of optically active states and spatially separated electron-hole pairs[4, 5]. For practical applications, one needs to produce large area heterojunctions of these materials. To achieve this goal, we have been investigating large area growth of these layered materials via atomic layer deposition (ALD). We report below on growth of WS_2 and SnS heterostructures, where both of the materials are layered metal chalcogenides, but of different crystal structures.

To date, axial MX_2 (where M = transition metal, X= S, Se or Te) heterostructures have been produced mostly by the mechanical transfer process of exfoliated layers. This approach has been utilized to fabricate devices that include p-n diodes[6-8], flexible MoS_2 transistors with graphene source/drain contacts[9] and MoS_2 semiconductor with h-BN insulator as a back-gated transistor[10], non-volatile memories[11], tunnel transistors[12], and top gated transistors composed of layers of MoS_2, h-BN, and graphene[13]. Although this approach has demonstrated the feasibility of producing heterostructures, it suffers from possibility of contamination, reproducibility, and lack of ability to scale up[3]. A technique that overcomes most of these limitations is chemical vapour deposition (CVD).

Growth of van der Waals heterostructures are well suited for CVD since these materials would not require lattice matching. This technique has been used to grow both lateral and vertical epitaxial layers of MoS_2 and WS_2, WSe_2 and $MoSe_2$, and mixed $MoS_2/MoSe_2$ and WS_2/WSe_2 heterostructures[14-16]. However, in all these cases the films are composed of triangular, faceted flakes. To overcome this limitation, we describe below growth of multilayered WS_2/SnS stacks of different thicknesses via ALD. Unlike CVD, these films were smooth and continuous as recently demonstrated with MoS_2 films[17].

[a] Department of Physics, Portland State University, Portland, OR
[b] Department of Electrical Engineering, University of Notre Dame, Notre Dame, IN

† Footnotes relating to the title and/or authors should appear here.
Electronic Supplementary Information (ESI) available: [details of any supplementary information available should be included here]. See DOI: 10.1039/x0xx00000x

ALD is a monolayer stepwise growth process where the reactants are alternately injected into the growth area, and following each reaction, excess species and by-products are purged out. As a result, high quality films are grown over large areas by sequential surface reactions[18]. This process enables precise control of the film composition and thickness as the growth proceeds layer by layer. Hence this approach is ideal for growth of layered materials and heterojunctions.

Experimental

The metal chalcogenide films were grown in a Microchemistry F-120 ALD reactor that can handle two 50 mm x 50 mm substrates per run. The substrates consisted of either p-or n-type Si wafers coated with a film of silicon oxide ranging in thickness from 55 nm to 940 nm. Initially, WS_2 and SnS films were grown separately at 390 ^{o}C. The precursors for WS_2 growth were WCl_5 and H_2S (9%, balance Ar). The WCl_5 source temperature was set at 110 ^{o}C and the carrier gas (nitrogen) flow rate was 250 sccm. The pulse sequence per cycle was as follows; WCl_5 pulse width was 0.8 s, N_2 purge of 1.0 s, H_2S pulse of 1.2 s, followed by 1.0 s N_2 purge. The film growth rate was 0.125 nm/cycle. Raman signal of a 2.5 nm thick WS_2 film (measured with AFM) produced with an excitation wavelength of 532 nm is shown in Fig. 1. This spectrum is similar to what has been reported in literature for the hexagonal lattice, 2H stacked phase[19]. The Raman spectrum is dominated by the first-order optical modes E^1_{2g} (355 cm^{-1}) and A_{1g} (418 cm^{-1}) and a second order longitudinal acoustic mode 2LA (M) at the M point, that occurs at 353 cm^{-1}. Since E^1_{2g} and the 2LA(M) modes are close together, they overlap[19, 20]. The peak at around 300 cm^{-1} is due to another 2LA(M)[20].

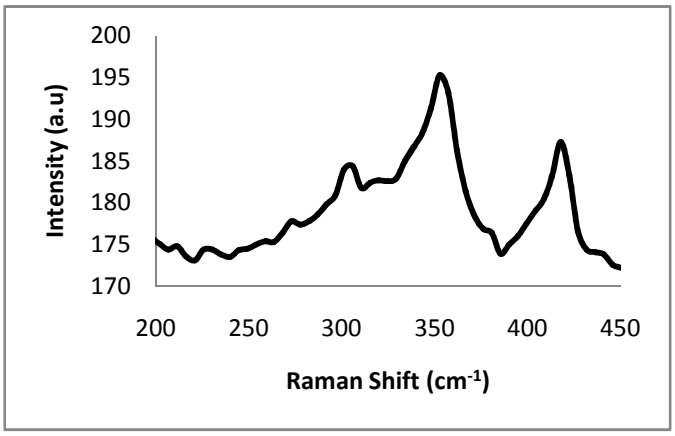

Figure1. Raman spectrum of WS_2 film.

The SnS films were grown from tin (II) acetylacetonate and H_2S. The tin source temperature was 95 ^{o}C and its pulse sequence was: tin 0.6 s, N_2 purge of 1 s, H_2S pulse of 1.2 s, and N_2 1 s. The growth rate was 0.47 nm/cycle. At lower growth temperatures (< 250 ^{o}C), the films were composed of mixed phases, however over around 300 ^{o}C, only SnS phase films were produced, as determined by Raman spectroscopy. Typical Raman spectrum from a 4.5 nm thick (measured via AFM) is shown in Fig. 2, where the laser pump wavelength was 532 nm. The peaks observed at 95, 162, 190, 225, and 287 cm^{-1} are consistent with those reported from single crystal SnS at 94, 162, 191, 219, and 288 cm^{-1}[20, 21]. The origin of these peaks has been attributed to first order single phonon oriented transverse or longitudinal optical vibrational modes[22].

The crystal structure of SnS has been described as orthorhombic with slightly distorted NaCl lattice[23]. However in contrast to a densely packed NaCl structure, it forms a layered structure with double layers perpendicular to the *a* axis, and where the layers are held by weak van der Waals bonds[23, 24]. The layered crystal structure and the unit cell of SnS are shown in Fig. 3.

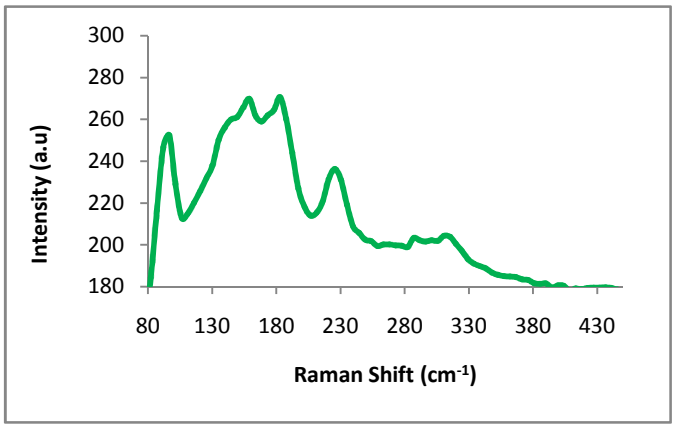

Figure2. Raman spectrum of SnS thin film.

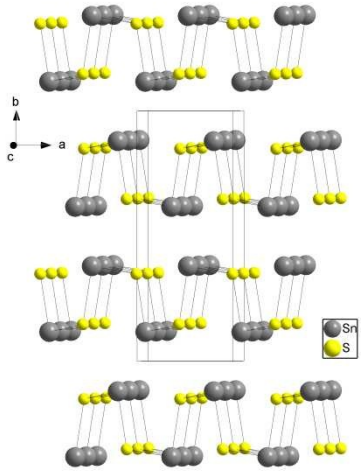

Figure 3. Crystal structure of the layered SnS film. The rectangular frame defines a unit cell. Striation direction is along the *b* axis. Space group is Pnma No. 62

Results and discussion

Heterojunctions were produced by alternately growing WS_2 and SnS layers. The thickness of each layer was controlled by selecting appropriate number of cycles of its precursors. Thickness of each material was varied from a couple of layers to 10 layers. The surface of these films was smooth and continuous. Scanning electron microscopy was employed to detect grain boundaries, but none was observed. Raman spectrum of one of these stacks is shown in Fig. 4. It shows the

two optical modes of WS_2 but not the LA(M) at 300 cm^{-1}. Both of these peaks are shifted towards higher frequency by 2 cm^{-1}.

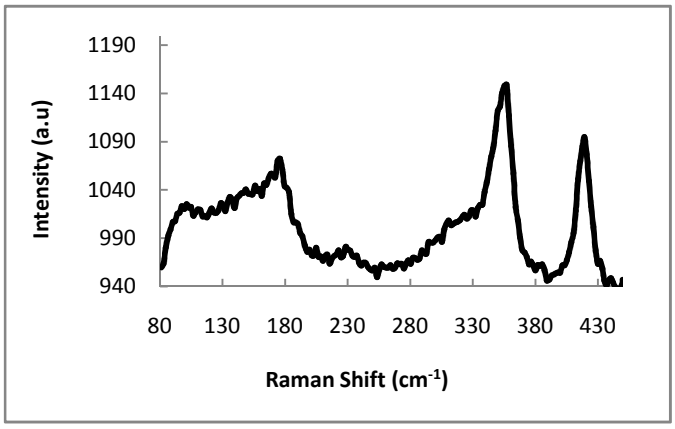

Figure 4. Raman spectrum of the WS_2/SnS hetrostructure.

After deposition, a small section of the sample of this stack was cleaved and saved for observation with a transmission electron microscope (TEM). The TEM samples were prepared using focused ion beam (FIB) milling which proved to be difficult since it damaged the films, especially the SnS layers. Hence, a sample composed of thicker films (Fig. 4) was selected for further analysis. A cross-sectional TEM view of a film composed of 3 pairs of SnS/WS_2layers is shown in Fig. 5.

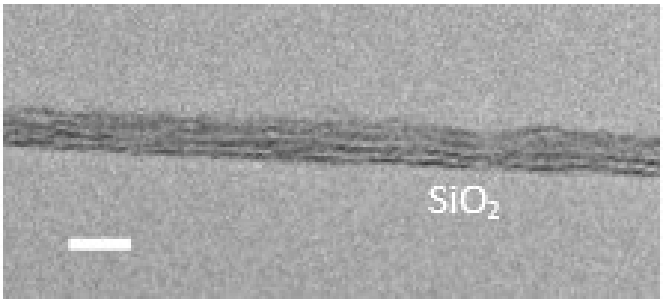

Figure 5. Cross-sectional TEM view of 3 alternating sets of WS_2 /SnS layers, starting with WS_2 at the bottom. Scale marker is 30nm.

This sample had the thickest SnS layer and suffered the least FIB damage, however the damage at the interface is evident. The low magnification micrograph is shown to demonstrate the continuous nature of the film. The darker layers are WS_2 and the lighter layers are SnS.

A close up of one of the WS_2/SnS interfaces from an undamaged portion is shown in Fig. 6, where a continuous transition can be observed from a layer of WS_2 to SnS. The four layers of WS_2 and the SnS lattice are clearly visible. These van der Waals materials were selected to study how they would align since they have different crystal structures.

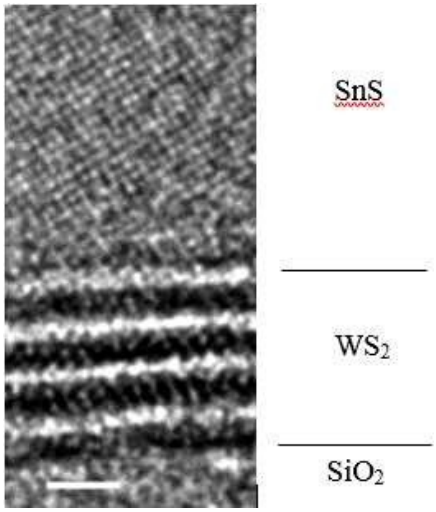

Figure 6. Cross-sectional TEM micrograph of the SnS/WS2 interface. The scale marker represents 1 nm.

The WS_2 displays a clear lattice only in the axial direction, where the spacing between the layers is measured to be about 6.2 Å. A comparison of this value with unstrained WS_2

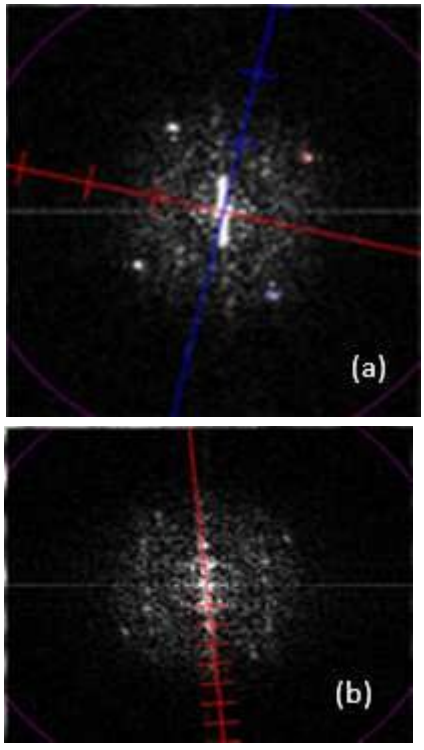

Figure 7. (a) FFT of SnS part of the structure. Lattice axes are shown on the FFT. Blue is the c* axis of SnS and red is the b* axis of SnS. (b) FFT of the WS_2 part of the structure.

(c=6.145 Å) [JCPDS 08-0237] confirms that the film is monophased and hexagonal. In the SnS portion, the peaks clearly visible in the FFT in figure 7a correspond to the {0,1,1} family of reflections, and thus the orientation corresponds to the [100] zone axis. The {0,0,1} reflections are not present due to reflection condition in Pnma group. The lattice parameters were determined to be c=4.06 Å, and a=4.36 Å, which matches with Herzenbergite SnS (JCPDS No. 39-0354, b= 3.9838 Å, c = 4.3291 Å). There is a stretch of about 2.2% in the b-direction and 0.6% in the c-direction.

It is interesting to note that although both WS_2 and SnS are layered materials, the Fast Fourier Transform analysis of the HRTEM images reveals that the orientation of SnS layers is completely different than the WS_2 layers. In order to reveal mutual orientation of the two lattices we took an FFT from the interface area. As can be seen from figure 8, the angle between c* (WS_2, green) and c* (SnS, blue) is close to 15 degrees. The closest low index zone axis, which corresponds to this tilt is the [410] axis, with angle to [001] being 14.03˚, thus the orientation relation between the two components of the heterostrucure is [410]SnS/[0001]WS2.This angular orientation continues at other interfaces in the stack. This is quite counterintuitive, since one would expect that two layered materials to pack in a way that preserves their layered structure within the heterostructure, as in the case of MoS_2/WS_2 heterojunctions, where stacked layers of MoS_2 and WS_2 preserved the 2H stacking[16]. In this case both the layers had similar 2H phase crystal structures[16]. However, in our case the two layered materials have different crystal structures where the layered nature of the materials is preserved, however the growth occurs at an angle with respect to their

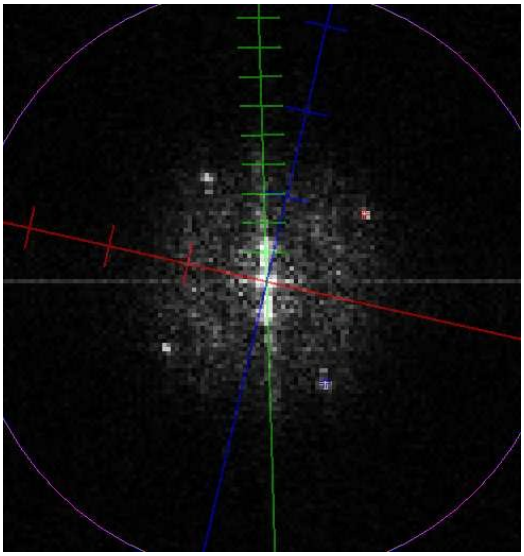

Figure 8. FFT of the interface section of figure 6. The green lattice corresponds to the WS_2 interlayer spacing. The blue c* axis of SnS, red b* axis of SnS.

van der Waals planes. This answers one of the questions we intended to address concerning heteroepitaxy of layered materials of different crystal structures.

The misaligned growth of the two materials would have implications on the electrical properties of the heterostructures. In order to better understand the effect of this orientation, back-gated transistors of WS_2, SnS, and the heterostructure were fabricated and characterized. The individual SnS and WS_2 devices were fabricated with films whose Raman signatures are presented in figures 1 and 2 and have thicknesses (4.5 nm and 2.5 nm respectively) roughly equal to those of the heterostructures shown in Fig. 5. Optical lithography was used to pattern source and drain contacts. This was followed by electron beam deposition of 30 nm of Ti, followed by 30 nm of Au for the WS_2 FETs and only Au film as the contact for SnS FETs. With the gate bias set at zero, the drain current versus drain voltage profiles were recorded. This showed a linear profile, indicating ohmic contacts. Next, the dependence of the drain current (Id) on the gate voltages (Vg) were examined. Field-effect mobility (μ) was extracted from slope of this curve in the linear region by using the expression

$$\mu = \frac{\Delta I_d}{V_g} \frac{L}{WV_d C}$$

, where V_d is the drain voltage (0.1 V), C is the gate capacitance per unit area, and L and W are the channel length and width, which were 6 μm and 100 μm, respectively[25]. The same procedure was then followed for the heterostructure films. Back-gated SnS transistors with Au contacts and gate oxide of 55 nm showed a p-type behaviour, with an effective mobility of 818 $cm^2 V^{-1} s^{-1}$. On the other hand, current transport in the WS_2 transistors with Ti/Au contacts is dominated by electrons, hence displayed an n-type transport with a mobility of 12 $cm^2 V^{-1} s^{-1}$. Plots of log of drain current (I_d) as a function of back gate voltage (V_g) for both these devices are shown in Fig. 9. The transfer characteristics of the heterojunction stack consisting of six layers composed of alternating 3 layers each of WS_2 and SnS (of Fig. 5) are shown in Fig. 10. It shows an ambipolar conductance, which was not surprising based on the individual transistors. For positive drain bias and gate voltage, it represents an n-FET while for negative drain bias and gate voltage it behaved as a p-FET. The effective mobilities, measured at room temperature, were 48 $cm^2 V^{-1} s^{-1}$ for n-FET and 20 $cm^2 V^{-1} s^{-1}$ for p-FET. While there is an increase in the mobility of WS_2, the p-type mobility of SnS drops. We attribute the significant drop in the hole mobility to the resistance of hole transport through the layer boundaries of SnS due to its alignment with respect to WS_2. This is consistent with the reported significant decrease in mobility of holes traveling from parallel to perpendicular direction of the van der Waals layers[26]. The I_{on}/I_{off} ratio for this device was 10^5. Also, since SnS is p-type and WS_2 is n-type, we expect a depletion region at the interface. This is one of the issues we plan to examine in the future.

Conclusions

We have utilized ALD to grow multiple heterojuctions composed of WS_2 and SnS layers over 5 cm x 5 cm silicon oxide coated silicon wafer substrates. The film surfaces were smooth and continuous. Cross-sectional TEM analysis showed that SnS layers grew at an angle of about 15 degrees with respect to WS_2 layers. This is most likely due to the different crystal structures of the two materials. Back-gated transistors showed that as a consequence of this misalignment, the hole mobility of SnS dropped significantly since the carriers had to pass through the van der Waals bonds. Currently, we are examining ALD grown heterojunctions of layered materials with similar crystal structures. We plan to report these results in the near future.

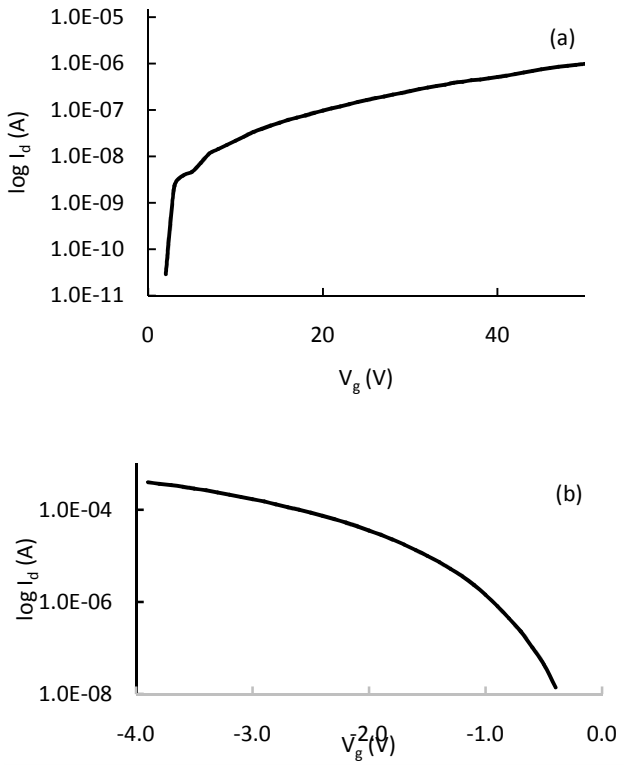

Fig. 9. Transfer characteristics of (a) WS_2 FET and (b) SnS FET.

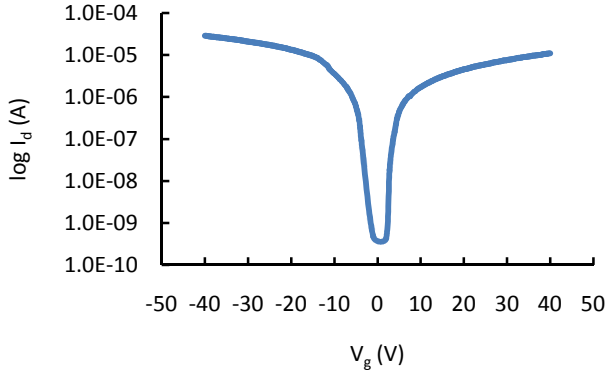

Fig. 10. Transfer characteristics of the heterojunction FET.

References

1 S. Z. Butler, S. M. Hollen, L. Cao, Y. Cui, J. A. Gupta, H. R. Gutiérrez, T. F. Heinz, S. S. Hong, J. Huang, A. F. Ismach, E. Johnston-Halperin, M. Kuno, V. V. Plashnitsa, R. D. Robinson, R. S. Ruoff, S. Salahuddin, J. Shan, L. Shi, M. G. Spencer, M. Terrones, W. Windl and J. E. Goldberger, *ACS Nano*, 2013, **7**, 2898-2926.
2 C. Ataca, H. Şahin and S. Ciraci, *The Journal of Physical Chemistry C*, 2012, **116**, 8983-8999.
3 A. K. Geim and I. V. Grigorieva, *Nature*, 2013, **499**, 419-425.
4 K. Kośmider and J. Fernández-Rossier, *Physical Review B*, 2013, **87**.
5 H. Terrones, F. Lopez-Urias and M. Terrones, *Sci Rep*, 2013, **3**, 1549.
6 R. Cheng, D. Li, H. Zhou, C. Wang, A. Yin, S. Jiang, Y. Liu, Y. Chen, Y. Huang and X. Duan, *Nano Lett*, 2014, **14**, 5590-5597.
7 B. W. Baugher, H. O. Churchill, Y. Yang and P. Jarillo-Herrero, *Nat Nanotechnol*, 2014, **9**, 262-267.
8 H. Fang, C. Battaglia, C. Carraro, S. Nemsak, B. Ozdol, J. S. Kang, H. A. Bechtel, S. B. Desai, F. Kronast, A. A. Unal, G. Conti, C. Conlon, G. K. Palsson, M. C. Martin, A. M. Minor, C. S. Fadley, E. Yablonovitch, R. Maboudian and A. Javey, *Proceedings of the National Academy of Sciences*, 2014, **111**, 6198-6202.
9 J. Yoon, W. Park, G. Y. Bae, Y. Kim, H. S. Jang, Y. Hyun, S. K. Lim, Y. H. Kahng, W. K. Hong, B. H. Lee and H. C. Ko, *Small*, 2013, **9**, 3295-3300.
10 G.-H. Lee, Y.-J. Yu, X. Cui, N. Petrone, C.-H. Lee, M. S. Choi, D.-Y. Lee, C. Lee, W. J. Yoo, K. Watanabe, T. Taniguchi, C. Nuckolls, P. Kim and J. Hone, *ACS Nano*, 2013, **7**, 7931-7936.
11 S. Bertolazzi, D. Krasnozhon and A. Kis, *ACS Nano*, 2013, **7**, 3246-3252.
12 L. Britnell, R. V. Gorbachev, R. Jalil, B. D. Belle, F. Schedin, A. Mishchenko, T. Georgiou, M. I. Katsnelson, L. Eaves, S. V. Morozov, N. M. R. Peres, J. Leist, A. K. Geim, K. S. Novoselov and L. A. Ponomarenko, *Science*, 2012, **335**, 947-950.
13 T. Roy, M. Tosun, J. S. Kang, A. B. Sachid, S. B. Desai, M. Hettick, C. C. Hu and A. Javey, *ACS Nano*, 2014, **8**, 6259-6264.
14 X. Duan, C. Wang, J. C. Shaw, R. Cheng, Y. Chen, H. Li, X. Wu, Y. Tang, Q. Zhang, A. Pan, J. Jiang, R. Yu, Y. Huang and X. Duan, *Nat Nanotechnol*, 2014, **9**, 1024-1030.
15 C. Huang, S. Wu, A. M. Sanchez, J. J. Peters, R. Beanland, J. S. Ross, P. Rivera, W. Yao, D. H. Cobden and X. Xu, *Nat Mater*, 2014, **13**, 1096-1101.
16 Y. Gong, J. Lin, X. Wang, G. Shi, S. Lei, Z. Lin, X. Zou, G. Ye, R. Vajtai, B. I. Yakobson, H. Terrones, M. Terrones, B. K. Tay, J. Lou, S. T. Pantelides, Z. Liu, W. Zhou and P. M. Ajayan, *Nat Mater*, 2014, **13**, 1135-1142.
17 R. Browning, P. Padigi, R. Solanki, D. J. Tweet, P. Schuele and D. Evans, *Materials Research Express*, 2015, **2**, 035006.
18 T. Suntola, *Materials Science Reports*, 1989, **4**, 261-312.
19 A. Berkdemir, H. R. Gutiérrez, A. R. Botello-Méndez, N. Perea-López, A. L. Elías, C.-I. Chia, B. Wang, V. H. Crespi, F. López-Urías, J.-C. Charlier, H. Terrones and M. Terrones, *Scientific Reports*, 2013, **3**.
20 W. Zhao, Z. Ghorannevis, K. K. Amara, J. R. Pang, M. Toh, X. Zhang, C. Kloc, P. H. Tan and G. Eda, *Nanoscale*, 2013, **5**, 9677-9683.
21 P. Sinsermsuksakul, J. Heo, W. Noh, A. S. Hock and R. G. Gordon, *Advanced Energy Materials*, 2011, **1**, 1116-1125.
22 H. R. Chandrasekhar, R. G. Humphreys, U. Zwick and M. Cardona, *Physical Review B*, 1977, **15**, 2177-2183.
23 N. K. Reddy, *ECS Journal of Solid State Science and Technology*, 2013, **2**, P259-P263.
24 J. H. Han, S. Lee and J. Cheon, *Chem Soc Rev*, 2013, **42**, 2581-2591.

25 W. Albers, C. Haas, H. J. Vink and J. D. Wasscher, *J. Appl. Phys.*, 1961, **32**, 2220.
26 M. Amani, M. L. Chin, A. G. Birdwell, T. P. O'Regan, S. Najmaei, Z. Liu, P. M. Ajayan, J. Lou and M. Dubey, *Applied Physics Letters*, 2013, **102**, 193107.